Korean J. Chem. Eng., 34(7), 2079-2085 (2017)
DOI: 10.1007/s11814-017-0090-5

pISSN: 0256-1115
eISSN: 1975-7220

Enhanced sunlight photocatalytic activity of silver nanoparticles decorated on reduced graphene oxide sheet

Moni Baskey (Sen)† and Sanjukta Ghosh

Materials Research Laboratory, Department of Chemistry, The University of Burdwan, Golapbag, Burdwan-713104, West Bengal, India
(*Received 13 December 2016 • accepted 26 March 2017*)

Abstract−A facile and straightforward method has been developed to synthesize silver nanoparticles decorated on reduced graphene oxide (RGO) nanosheets through hydrothermal reaction. The composite was characterized by XRD, UV-Visible spectroscopy, SEM and TEM techniques. In this synthesized RGO-Ag nanocomposite, the Ag nanoparticles size ranges 30-50 nm. Moreover, the RGO-Ag composites exhibited excellent photocatalytic activity towards the degradation of methylene blue (MB) in presence of sunlight. This photocatalytic reaction is completed within 20 min and the rate of reaction depends on the amount of RGO present in the nanocomposites.

Keywords: RGO-Ag Nanocomposite, Hydrothermal Synthesis, Photocatalytic Degradation, Methylene Blue, Photostability

INTRODUCTION

In the carbon family, graphene has become a rising star because of its excellent electronic [1], conductive [2], mechanical properties [3], superior chemical stability [4] and high specific surface area [5] as well as its potential applications in photocatalysis [6-9], catalysis [10,11] energy storage [12-14] and solar fuels [15]. The inherent properties of metal nanoparticles (NPs) can be enhanced by using a support such as graphene [16-18], since graphene sheets have the unique ability to promote fast electron-transfer kinetics for a wide range of electro active species. Thus, metal-graphene composite materials have been widely used in different applications [19,20] because of their high surface area, stability under ambient conditions and faster electron-transport mechanism [6]. Improved catalytic activities of several metal NPs supported on reduced graphene oxide (RGO) have been reported recently [21-27]. Graphene oxide enwrapped metal/metal halide nanocomposite also has been shown active photocatalyst under visible-light irradiation [28].

Nowadays, environmental pollution is a main issue and harmful organic chemical compounds are often discharged with wastewater into the surface water without adequate treatment, which has become the main cause of water pollution. Rapid and convenient removal of organic chemical compounds from waste water has been a challenging issue [29-31]. Silver nanoparticles are environmentally friendly, biocompatible and have been used for removal of organic dye from wastewater [32-34]. The bulk materials at micrometer regime show very poor catalytic property and weak interaction between adsorbate and adsorbent due to the poor surface area [35]. Because of high surface area (2,600 $m^2 g^{-1}$) of graphene, it became a very potential candidate among existing carbon-based derivatives [36] for environment application.

Here, we have evaluated the hydrothermal method for the synthesis of RGO-Ag nanocomposite which acts as an efficient photocatalyst. The as-synthesized nanocomposite has been characterized by XRD, TGA, TEM, SEM, DLS, UV spectroscopic analysis and photoluminescence study. The catalytic activity of the RGO-Ag nanocomposite has been investigated by studying the photocatalytic degradation of an aqueous solution of methylene blue (MB) under sunlight irradiation.

EXPERIMENTAL SECTION

1. Materials

The materials consisted of ultrafine graphite powder (Aldrich), potassium permanganate (Merck), conc. sulfuric acid (Merck, 98% pure), hydrogen peroxide (30%, Merck), hydrochloric acid (30%, Merck), silver nitrate (Merck), hydrazine hydrate (Merck), methylene blue (MB), doubled distilled water.

2. Synthesis of RGO-Ag Nanocomposite

Graphene oxide (GO) was prepared from graphite powder following the Hummers method [37]. At first, GO dispersion (0.01 g mL^{-1}) was taken and sonicated to get clear dispersion. To it, 5 ml of 0.1209 (M) $AgNO_3$ was added and stirred for 30 minutes to get GO-Ag dispersion. This dispersion became muddy color after the addition of 5 ml of hydrazine hydrate and stirring for 30 minutes. After the completion of stirring, it was washed by centrifuge with double distilled water, transferred to 100 ml Teflon lined autoclave and hydrothermally treated at 120 °C for 8 hours. At the end of the reaction, black product was obtained and washed several times with double distilled water, followed by ethanol to remove the impurities and dried at 60 °C under vacuum condition. The same procedures were followed to prepare RGO and Ag nanoparticles (A) in the absence of $AgNO_3$ and RGO, respectively. The weight ratios of the GO and $AgNO_3$ are given in Table 1.

3. Characterization

Structural morphology was investigated by scanning electron

†To whom correspondence should be addressed.
E-mail: moni.baskey@gmail.com

Table 1. Weight ratios of $AgNO_3$ and GO used for the preparation of RGO-Ag

Sample	Amount of $AgNO_3$ (g)	Amount of GO (g)	Weight ratio (AgNO : GO)
AG1	0.1027	0.1048	1 : 1
AG4	0.1026	0.4192	1 : 4
AG8	0.1027	0.8208	1 : 8
RGO	-	0.205	-
A	0.1027	-	-

microscope [JSM6700F (JEOL, Tokyo, Japan)], and the microstructure of the as-synthesized samples was studied by transmission electron microscope (Model JEOL-2011). Powder X-ray diffraction (XRD) measurement was carried out using powdered sample with an X-ray diffractometer (RICH SEIFERT-XRD 3000P with X-ray Generator-Cu, 10 kV, 10 mA, wavelength 1.54 Å), and thermogravimetric analysis (TGA) was conducted by SDT Q600 V20.5 Build 15 in the temperature range 298 K to 973 K at a heating rate 5 K/min throughout the experiment. Dynamic light scattering (DLS) study for size distribution measurement of the Ag nanoparticles was made by dynamic light scattering (Model DLS-nano ZS, Zetasizer, Nanoseries, Malvern Instruments) and photoluminescence study was done by Horiba Fluoromax QM400. The UV-vis spectra and the photocatalytic experiments were investigated by SHIMADZU UV-1800 spectrophotometer.

4. Photocatalytic Study

The photocatalytic performance of the prepared RGO-Ag nanocomposites was carried out with methylene blue (MB) dye under natural sunlight irradiation. All the prepared photocatalyst materials (10 mg) were separately dispersed in 50 mL of MB solution (12 mg L^{-1}) under stirring condition and kept in dark environment for 30 min to get well adsorption-desorption equilibrium. After the sunlight irradiation, at given time intervals, 3 mL of irradiated MB dye solution was periodically withdrawn and the transparent solution was separated by centrifugation. The concentration of MB dye in the reaction solution for each sample was determined with a UV-visible absorption spectrophotometer, by measuring the absorbance intensity at 664 nm during the photocatalytic degradation process. Concentration of dye during degradation was calculated by the absorbance value at 664 nm. Percentage of dye degradation was estimated by the following formula:

$$\% \text{ De-colorization} = 100 \times (A_0 - A_t)/A_0, \quad (1)$$

where A_0 is the initial absorbance of dye solution and A_t is the absorbance of dye solution after photocatalytic degradation.

RESULTS AND DISCUSSION

1. X-ray Diffraction Study of the RGO-Ag Composite

The crystal structure of the composite was characterized by X-ray diffraction study. In Fig. 1(b), the X-ray diffraction peak of RGO at 2θ~26° is for the (002) plane of graphene sheet. But in case of the composite shown in Fig. 1(a), the diffraction peaks at around 38.1, 44.4 and 64.5 for the (111), (200), and (220) planes of Ag nanoparticles, respectively. In addition, the hump between 17° and 27° is shown which became broadened and left shifted compared with the corresponding peak for graphene. The broad nature of the peak indicates poor ordering of the sheets along the stacking direction. The left shifting of the (002) peak confirms that the silver nanoparticles were embedded between the layers [38,39], which also supported by SEM images (Fig. 3(a)).

2. UV-vis Spectroscopy

To understand the successful formation of RGO-Ag composite, a UV-vis study was conducted of GO, the sample before and after hydrothermal reaction. From Fig. 1(c), it was shown that GO shows two absorbance peaks at 230 nm and 305 nm corresponding to π-π* transitions of aromatic C=C bond and n-π* transitions of C=O bond in GO, respectively (black line). It is clearly seen that the absorption peak gradually red-shifted from 230 to 238 and finally to 265 nm for GO-Ag and RGO-Ag composites. In addition, a new absorption band appears at 457 nm ascribed to the colloidal silver surface plasmon resonance band, indicating the formation of GO-Ag composite in bulk phase. But after the completion of reaction, this spectrum blue-shifted to 427 nm, which is a clear indication for the formation of graphene-Ag composite in nanophase, and also band gap increases than bulk phase.

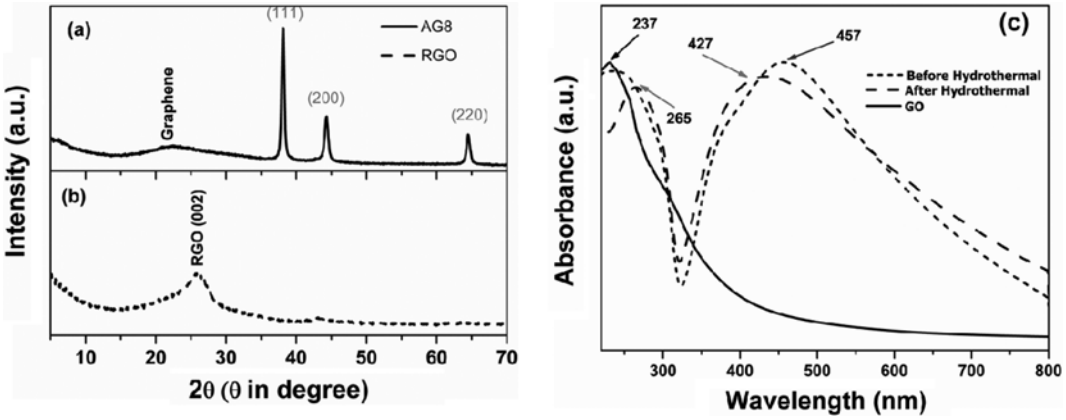

Fig. 1. (a) and (b) XRD patterns of RGO-Ag nanocomposite and RGO (c) UV plots of GO and the RGO-Ag composite (before and after hydrothermal reaction).

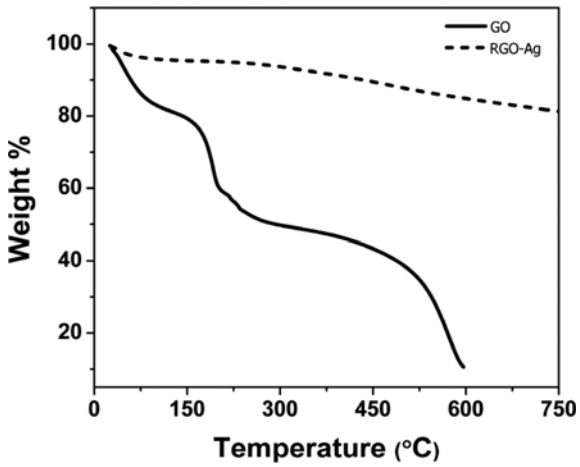

Fig. 2. TGA of GO and RGO-Ag nanocomposite.

The band gap of the silver nanoparticles on graphene is calculated on the basis of the formulae as given below:

$$Eg\ (eV)=1240/\lambda$$

which comes out to be 2.9 eV after hydrothermal reaction from the bulk phase (2.71 eV) [40].

3. Thermogravimetric Analysis (TGA)

In Fig. 2, the TGA curves show the successful functionalization of reduced graphene oxide sheets with Ag nanoparticles. RGO-Ag composite shows much higher thermal stability than the GO. There is a mass loss (~10%) below 100 °C attributed to the removal of adsorbed water and the main weight loss takes place around 150-500 °C due to pyrolysis of the labile oxygen-containing functional groups, since GO has a layered morphology with oxygen containing functional groups which will disrupt the hexagonal carbon basal planes on thermal heating, thus accelerating the process of weight loss. Compared with GO, the weight loss of the RGO-Ag composite up to 750 °C is much lower, indicating that GO has been converted into RGO after reduction.

4. SEM and TEM Micrograph Study

The morphology of the composite was observed by SEM. Fig. 3(a) and 3(b), which displays the typical SEM images of RGO-Ag nanocomposite. The RGO-Ag nanocomposite exhibits a uniform decoration of Ag nanoparticles on both sides of the RGO sheets. The average size of Ag nanoparticles is about 40 nm. The distribution of Ag nanoparticles on the RGO sheet surface prevents the restacking phenomenon of RGO sheets.

The size, shape and morphology of the silver nanoparticles grown on RGO surface were studied by transmission electron microscopy (TEM). The TEM image (Fig. 3(c)) shows that the Ag nanoparticles are almost spherical with an average diameter of 30-50 nm. High-resolution TEM (HRTEM) image in Fig. 3(d) exhibits clear lattice fringes of samples, which confirms that the nanoparticles are highly crystalline with an interplanar spacing of 0.205 nm that can be attributed to the (200) planes of silver nanoparticles of (JCPDS no 04-0783).

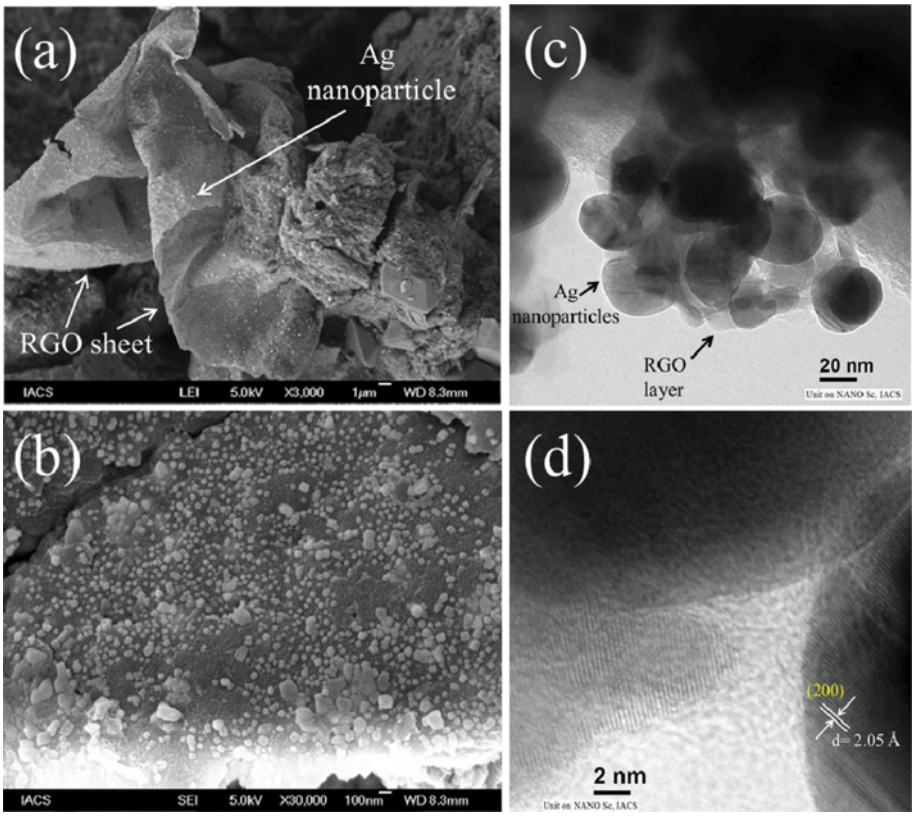

Fig. 3. (a) and (b) SEM images of RGO-Ag nanocomposite, (c) and (d) TEM image of the RGO-Ag nanocomposite and HRTEM of (c).

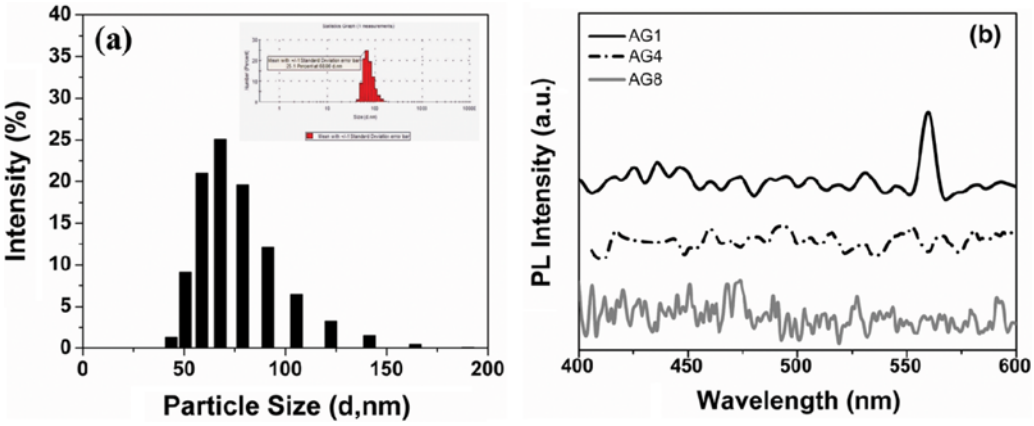

Fig. 4. (a) DLS study for the measurement of average size distribution of Ag nanoparticles (b) Room temperature photoluminescence spectra of bare RGO-Ag nanocomposites (AG1, AG4, and AG8).

5. DLS Study

The DLS study for measurement of average size distribution of Ag nanoparticles is shown in Fig. 4(a). It is clear that the average particle size is 68 nm. But in the TEM micrograph [Fig. 3(c)] of the nanocomposite, the average particle size is 30-50 nm. The decrease in particle size is due to the incorporation of RGO as a growing support into Ag nanoparticles [41].

6. Photoluminescence Study

The photoluminescence study of the material is related to the surface states which determine the efficiency of migration and transfer of charge carriers and also supply information such as oxygen vacancies and defects as well as the separation and recombination of photo-induced charge carriers [42,43]. The PL spectrum intensity is an indicator to the number of electron-hole recombination centers present in the material. Therefore, the luminescence properties were examined to determine the optical properties of the RGO-Ag nanocomposites as shown in Fig. 4(b). In the spectrum, the PL intensity of AG1 is higher due to having less RGO content in the composite, and the luminescence intensity decreases with increasing the RGO content in the RGO-Ag nanocomposites, which indicates the electron-hole pair recombination in Ag nanoparticles inhabited in the higher RGO content nanocomposites and decreases the PL intensity. The inhibition effect is due to the combination of RGO into Ag nanoparticles, which plays an important role in the photocatalytic performance in the RGO-Ag nanocomposites.

7. Formation Mechanism

To explain the formation of silver nanoparticles on graphene surface in the present case as shown in Scheme 1, different experiments such as XRD, SEM and TEM studies have been done. GO is anchored by several negatively reactive sites for chemical modi-

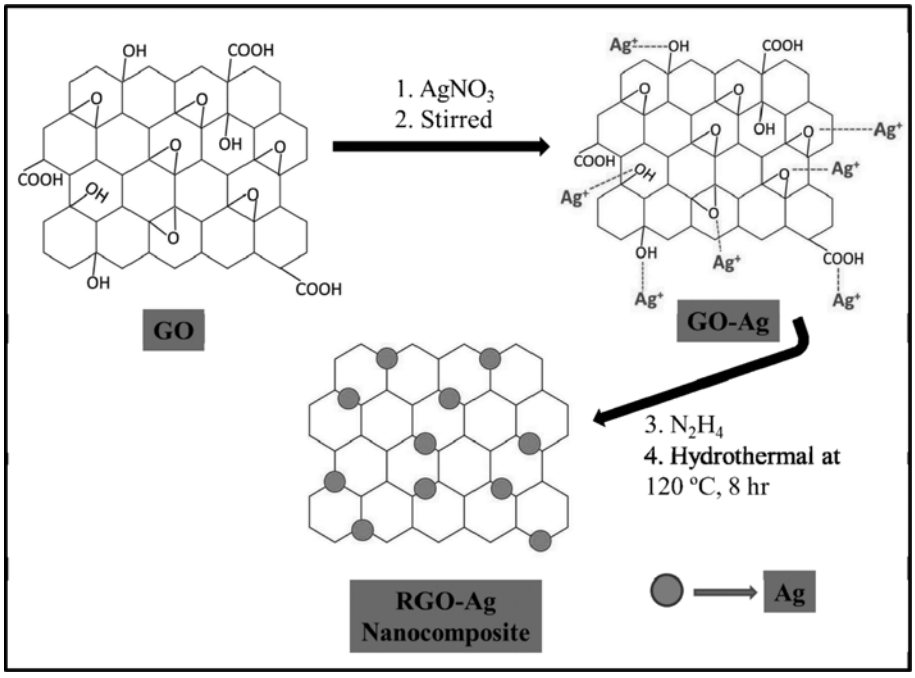

Scheme 1. Plausible formation mechanism of Ag nanoparticles on RGO sheet.

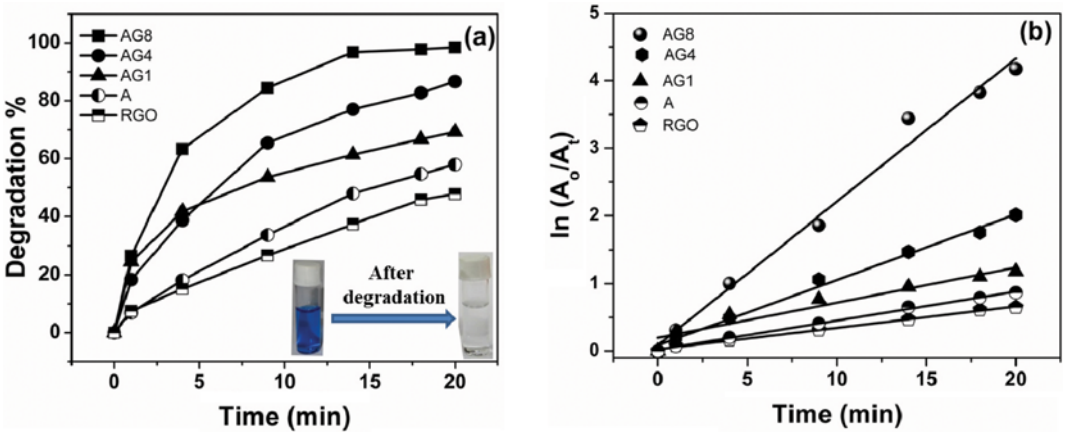

Fig. 5. (a) and (b) Photocatalytic degradation of MB and rate kinetics in the presence of different photocatalysts under sunlight irradiation.

fication of the carbon network by grafting atoms or molecules [44]. After the addition of $AgNO_3$ solution, Ag^+ ions are coordinated with them by electrostatic interaction due to numerous numbers of oxygenated groups like hydroxyl, epoxy and carboxylic acid on GO sheets [45]. It is reported that, GO and Ag^+ get reduced to graphene [46] and Ag [47], respectively, on the addition of hydrazine hydrate. Thus, Ag nanoparticles are grown on RGO surface.

8. Photocatalytic Study of RGO-Ag Composites

The photocatalytic performance of the prepared photocatalytic materials, RGO, RGO-Ag nanocomposites were separately evaluated for the degradation of a methylene blue (MB) dye under sunlight irradiation. The results of the photo-degradation study are shown in Fig. 5(a). The initial concentration of MB decreases with irradiation time and the rate of photo-degradation strongly depends on the presence of the light and of the catalyst. The presence of catalyst initiates the degradation of MB under visible light. Most interestingly, the visible-light-induced degradation of MB by RGO-Ag is most effective compared to degradation by Ag nanoparticle or RGO individually. During the photocatalytic experiments, Ag nanoparticles and RGO achieved only 58% and 47% photodegradation after 20 min of sunlight irradiation (Fig. 5(a)). The poor photocatalytic performance of the Ag nanoparticles can be explained by the aggregation of Ag nanoparticles, which leads to the formation of larger particles due to Ostwald repining process [48]. Interestingly, a maximum photodegradation of MB was observed at 20 min light irradiation when a photocatalyst of Ag nanoparticles combined with reduced graphene oxide sheets was used. To optimize the RGO content for maximum photo-degradation of MB dye, photocatalytic experiments were performed with different compositions of RGO.

The higher the content of RGO in the nanocomposites, the higher the oxygen containing groups. Hence, AG1 contains the lowest amount of RGO, which offers fewer active sites for the adsorption of MB molecules on RGO sheets. This favors the facile transport of photo-excited electrons to reach the surface reaction sites more easily [49], and thereby efficiently inhibits the recombination of photo-induced electron-hole pairs during the electron transfer process. Among the photocatalysts, AG8 exhibited excellent photocatalytic activity; almost 98% of the MB was decolorized in 20 min where AG4 and AG1 show 86% and 69% degradation ability in the same time duration. Meanwhile, the bare Ag nanoparticles photocatalyst could achieve only 58% MB dye removal efficiency. This suggests that Ag nanoparticles grown on RGO surface enhance the photocatalytic activity for the dye degradation under sunlight irradiation.

Fig. 5(b) shows the plot $\ln(A_o/A_t)$ as a function of time where, A_o is the absorbance at t=0 and A_t the absorbance at time t=t. It is clear that the reaction follows pseudo first-order kinetics [50] and corresponding rate constants were calculated to be 0.2117, 0.096, 0.0520, 0.0317 and 0.043 min^{-1} in case of AG8, AG4, AG1, RGO nanocomposite and bare silver nanoparticles, respectively, which indicates that the rate of reaction is enhanced in the presence of the reduced graphene oxide surface.

9. Recyclability Test

The photo-stability of RGO-Ag nanocomposite was investigated by recyclability experiment. After each cycle of photodegradation test, the photocatalyst was separated from MB solution by centrifugation, washed with water, dried in vacuum and the same volume of fresh MB solution was added for the next cycle. The results of the recyclability test are shown in Fig. 6. The photocata-

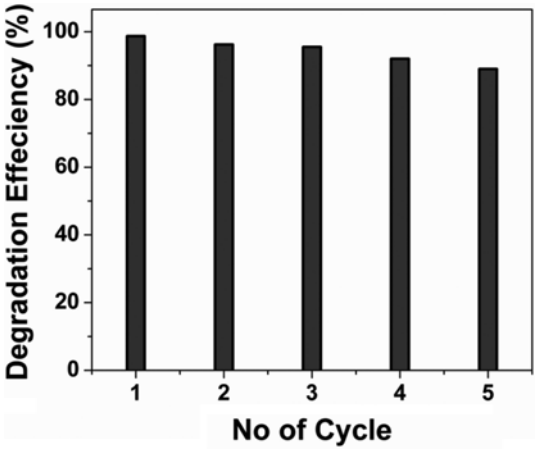

Fig. 6. Recyclability test of RGO-Ag nanocomposite.

lyst exhibits excellent photostability even after five cycles, which further confirms that RGO-Ag nanocomposites have excellent stability under sunlight irradiation.

10. Mechanism of Enhanced Photocatalysis for the Photodegradation Performance of MB

This photocatalytic phenomenon was explained on the basis of use of RGO as the catalyst support leads to a synergistic effect, which might be helpful for the increase of catalytic activity. The synergistically enhanced catalytic activity due to absorption of MB molecules on graphene sheet can be explained as follows: there are several oxygen atoms on GO due to presence of epoxy, hydroxyl, and carboxyl groups, which are highly amenable to positively charged molecules because of strong electrostatic interactions [44]. But, also in RGO, the number of oxygen atoms is quite lower than that of GO, but there might be π-π stacking interaction. MB molecules are positively charged, so the electrostatic interaction between the RGO and the MB molecules is the primary binding strength. It was expected that MB could be adsorbed onto the surface of RGO via π-π stacking interaction, providing a higher MB concentration near the Ag nanoparticles on the surface of RGO (green dotted arrow in Scheme 2), and therefore leading to more efficient contact between them.

A probable photocatalytic mechanism for the RGO-Ag nanocomposite was proposed based on the above photocatalytic analysis and presented in Scheme 2. So, during exposure in sunlight, when the photons hit the nanoparticles present in the colloidal mixture, the electrons at the particle surface are excited [51], and the excited electrons (e^-) from the valence band (VB) of Ag nanoparticle move to its conduction band (CB), leaving holes in the VB, thereby forming the electron-hole pairs [52]. The photogenerated electrons from the conduction band can transfer rapidly to the graphene surface due to the intimate contact between the Ag nanoparticles and RGO surface, resulting in a significantly improved lifetime of the photogenerated electron-hole charge carrier. Due to having high charge carrier mobility of graphene, RGO could act as an electron acceptor and transporter to prevent the recombination rate of the photogenerated electron-hole pairs [53-55].

The electrons then convert the dissolved oxygen molecules in the reacting medium into oxygen anion radicals, and at the same time the holes can react with adsorbed water to produce hydroxyl radicals ($^{\cdot}OH$) [56,57]. These radicals break MB molecules into organic molecules which results in the rapid degradation of the dye. Therefore, RGO-Ag nanocomposite may act as a stable and efficient photocatalyst for the degradation of MB under sunlight irradiation.

CONCLUSION

We have successfully designed and synthesized RGO-Ag nanocomposites that act as a novel photocatalyst. The XRD, UV-visible spectroscopy and morphological studies revealed strong interactions between Ag nanoparticles and RGO. RGO-Ag nanocomposite exhibited higher activity for the degradation of MB under sunlight irradiation within 20 min and the photocatalytic activity increases with the increase of RGO amount.

ACKNOWLEDGEMENT

M.B.S is thankful for financial support by Burdwan University Research Grant (Ref No. RTI/ULRC/130). S.G. acknowledges the Bazar Bonkapasi S.M. High School, Burdwan for giving permission to continue her research work. We acknowledge Mr. Diptiman Dinda, IACS, Kolkata, for XRD and PL instrumental facility. We also acknowledge Ms. Somashree Kundu, UGC-DAE CSR,

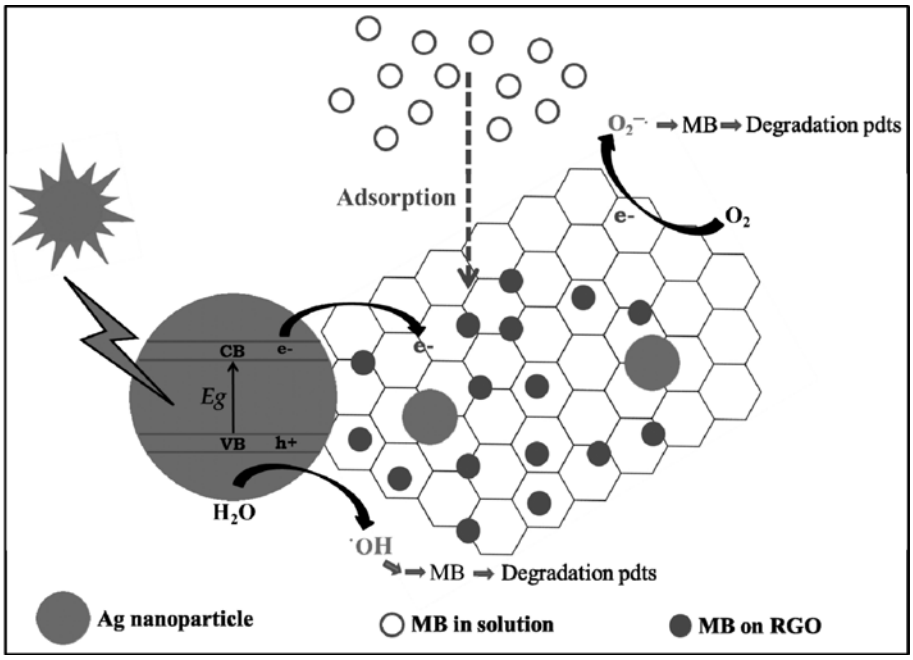

Scheme 2. A schematic representation of photocatalytic mechanism.

Kolkata for DLS instrumental facility.

REFERENCES

1. K. I. Bolotin, K. J. Sikes, Z. Jiang, M. Klima, G. Fudenberg, J. Hone, P. Kim and H. L. Stormer, *Solid State Commun.*, **146**, 351 (2008).
2. A. A. Balandin, S. Ghosh, W. Bao, I. Calizo, D. Teweldebrhan, F. Miao and C. N. Lau, *Nano Lett.*, **8**, 902 (2008).
3. C. Lee, X. Wei, J. W. Kysar and J. Hone, *Science*, **321**, 385 (2008).
4. A. K. Geim, *Science*, **324**, 1530 (2009).
5. A. Peigney, Ch. Laurent, E. Flahaut, R. R. Bacsa and A. Rousset, *Carbon*, **39**, 507 (2001).
6. Q. Xiang, J. Yu and M. Jaroniec, *Chem. Soc. Rev.*, **41**, 782 (2012).
7. X. An and J. C. Yu, *RSC Adv.*, **1**, 1426 (2011).
8. Z. Xiong, L. Zhang, J. Ma and X. S. Zhao, *Chem. Commun.*, **46**, 6099 (2010).
9. P. Roy, A. P. Periasamy, C.-T. Liang and H.-T. Chang, *Environ. Sci. Technol.*, **47**, 6688 (2013).
10. Y. Li, W. Gaob, L. Ci, C. Wang and P. M. Ajayan, *Carbon,* **48**, 1124 (2010).
11. J. Huang, L. Zhang, B. Chen, N. Ji, F. Chen, Y. Zhang and Z. Zhang, *Nanoscale*, **2**, 2733 (2010).
12. L. Peng, Y. Zhu, H. Li and G. Yu, *Small,* **12**, 6183 (2016).
13. X. Zhang, L. Hou, A. Ciesielski and P. Samorì, *Adv. Energy Mater.*, **6**, 1600671 (2016).
14. Z. Protich, P. Wong and K. S. V. Santhanam, *ACS Sustainable Chem. Eng.*, **4**, 6177 (2016).
15. J. Low, J. Yu and W. Ho, *J. Phys. Chem. Lett.*, **6**, 4244 (2015).
16. Y. Nishina, J. Miyata, R. Kawai and K. Gotoh, *RSC Adv.,* **2**, 9380 (2012).
17. S. J. Zhen, W. L. Fu, B. B. Chen, L. Zhan, H. Y. Zou, M. X. Gao and C. Z. Huang, *RSC Adv.*, **6**, 93645 (2016).
18. L. Yan, Y.-N. Chang, W. Yin, G. Tian, L. Zhou, Z. Hu, G. Xing, Z. Gu and Y. Zhao, *Adv. Eng. Mater.*, **17**, 523 (2015).
19. J. Wang, X. B. Zhang, Z. L. Wang, L. M. Wang and Y. Zhang, *Energy Environ. Sci.,* **5**, 6885 (2012).
20. S. Pattnaik, K. Swain and Z. Lin, *J. Mater. Chem. B*, **4**, 7813 (2016).
21. S. Moussa, A. R. Siamaki, B. F. Gupton and M. S. El-Shall, *ACS Catal.,* **2**, 145 (2012).
22. N. Zhang, M.-Q. Yang, S. Liu, Y. Sun and Y.-J. Xu, *Chem. Rev.*, **115**, 10307 (2015).
23. C. Han, N. Zhang, Y.-J. Xu, *Nano Today,* **11**, 351 (2016).
24. M.-Q. Yang, N. Zhang, M. Pagliaro and Y.-J. Xu, *Chem. Soc. Rev.*, **43**, 8240 (2014).
25. M.-Q.Yang, C. Han, N. Zhang and Y.-J. Xu, *Nanoscale*, **7**, 18062 (2015).
26. K.-Q. Lu, N. Zhang, C. Han, F. Li, Z. Chen and Y.-J. Xu, *J. Phys. Chem. C*, **120**, 27091 (2016).
27. N. Zhang, M.-Q. Yang, Z.-R. Tang and Y.-J. Xu, *ACS Nano*, **8**, 623 (2014).
28. M. Zhu, P. Chen and M. Liu, *Acs Nano*, **5**, 4529 (2011).
29. M. Boller, *Water Sci. Technol.,* **35**, 1 (1997).
30. M. O. Awaleh and Y. D. Soubaneh, *Hydrol. Current Res.*, **5**, 1000164 (2014).
31. L. Nelik and M. Zarreii, Wastewater treatment: present challenges, future horizons, Water & Wastes Digest, February 15 (2010).
32. S. Bhakya, S. Muthukrishnan, M. Sukumaran, M. Muthukumar, T. S. Kumar and M. V. Rao, *J. Bioremed. Biodeg.*, **6**, 1000312 (2015).
33. Z.-C.Wua, Y. Zhanga, T.-X. Taoa, L. Zhang and H. Fong, *Appl. Surf. Sci.*, **257**, 1092 (2010).
34. S. R. Kavitha, M. Umadevi, S. R. Janani, T. Balakrishnan and R. Ramanibai, *Spectrochim. Acta Mol. Biomol. Spectrosc.*, **127**, 115 (2014).
35. S. Chaturvedia, P. N. Dave and N. K. Shah, *J. Saudi Chem. Soc.*, **16**, 307 (2012).
36. J. G. Radich, A. L. Krenselewski, J. Zhu and P. V. Kamat, *Chem. Mater.*, **26**, 4662 (2014).
37. W. S. Hummers and R. E. Offeman, *J. Am. Chem. Soc.,* **80**, 1339 (1958).
38. S. Sharma, A. Ganguly, P. Papakonstantinou, X. Miao, M. Li, J. L. Hutchison, M. Delichatsios and S. Ukleja, *J. Phys. Chem. C*, **114**, 19459 (2010).
39. L. I. Sanlı, V. Bayram, B. Yarar, S. Ghobadi and S. A. Gűrsel, *Int. J. Hydrogen Energy,* **41**, 3414 (2016).
40. H. Kumar and R. Rani, *International Journal of Engineering and Innovative Technology*, **3**, 344 (2013).
41. R. T.-Mendieta, D. V.-Espinosa, S. Sabater, J. Lancis, G. M.-Vega and J. A. Mata, *Sci. Rep.*, **6**, 30478 (2016).
42. Y. Cong, J. Zhang, F. Chen and M. Anpo, *J. Phys. Chem. C*, **111**, 6976 (2007).
43. X. Chen, X. Wang, Y. Hou, J. Huang, L. Wu and X. Fu, *J. Catal.*, **255**, 59 (2008).
44. S. Chen, J. Zhu, X. Wu, Q. Han and X. Wang, *ACS Nano*, **4**, 2822 (2010).
45. K. S.-Stanek, A. Kisielewska, J. Ginter, K. Bałuszynska and I. Piwonski, *RSC Adv.*, **6**, 60056 (2016).
46. M. J. Fernández-Merino, L. Guardia, J. I. Paredes, S. Villar-Rodil, P. Solís-Fernández, A. Martínez-Alonso and J. M. D. Tascón, *J. Phys. Chem. C.*, 1**14**, 6426 (2010).
47. V. V. Tatarchuk, A. P. Sergievskaya, T. M. Korda, I. A. Druzhinina and V. I. Zaikovsky, *Chem. Mater.*, **25**, 3570 (2013).
48. W. Ostwald, *Z. Phys. Chem.*, **34**, 495 (1900).
49. T. See, A. Pandikumar, L. Ngee, H. Ming and C. Hua, *Catal. Sci. Technol.*, **4**, 4396 (2014).
50. T. Chen, Y. Zheng, J. Lin and G. Chen, *J. Am. Soc. Mass Spectrom.*, **19**, 997 (2008).
51. K. Roy, C. K. Sarkar and C. K. Ghosh, *Appl. Nanosci.*, **5**, 953 (2015).
52. Z. Ren, J. Zhang, F. X. Xiao and G. Xiao, *J. Mater. Chem. A*, **2**, 5330 (2014).
53. Y. Aihua, F. Wenqing, Z. Qinghong, D. Weiping and W. Ye, *Catal. Sci. Technol.*, **2**, 969 (2012).
54. N. Jiang, Z. Xiu, Z. Xie, H. Li, G. Zhao, W. Wang, Y. Wu and X. Hao, *New J. Chem.*, **38**, 4312 (2014).
55. X. Wang, H. Tian, Y. Yang, H. Wang, S. Wang, W. Zheng and Y. Liu, *J. Alloy. Compd.*, **524**, 5 (2012).
56. Y. Zhang, N. Zhang, Z.-R. Tang and Y.-J. Xu, *J. Phys. Chem. C*, **118**, 5299 (2014).
57. Z.-R. Tang, Y. Zhang, N. Zhangab and Y.-J. Xu, *Nanoscale*, **7**, 7030 (2015).